Dynamics of a mutual inhibition circuit between pyramidal neurons compared to human perceptual competition

Article (Accepted Version)

JNeurosci
THE JOURNAL OF NEUROSCIENCE

Research Articles: Systems/Circuits

Dynamics of a mutual inhibition between pyramidal neurons compared to human perceptual competition

https://doi.org/10.1523/JNEUROSCI.2503-20.2020

Cite as: J. Neurosci 2020; 10.1523/JNEUROSCI.2503-20.2020

Received: 23 September 2020
Revised: 16 November 2020
Accepted: 9 December 2020

Title

Dynamics of a mutual inhibition between pyramidal neurons compared to human perceptual competition

Abbreviated title

MUTUAL-INHIBITION-IN-A-DISH

Authors/Affiliations

N. Kogo (corresponding author)
Biophysics, Donders Institute for Brain, Cognition and Behaviour, Radboud University, The Netherlands
F. B. Kern
School of Life Sciences, Sussex Neuroscience, University of Sussex, United Kingdom
T. Nowotny
School of Engineering and Informatics, University of Sussex, United Kingdom
R. van Ee
Biophysics, Donders Institute for Brain, Cognition and Behaviour, Radboud University, The Netherlands
Brain and Cognition, University of Leuven, Belgium
R. van Wezel
Biophysics, Donders Institute for Brain, Cognition and Behaviour, Radboud University, The Netherlands
Biomedical Signals and Systems, MedTech Centre, University of Twente, The Netherlands
T. Aihara
Graduate School of Brain Sciences, Tamagawa University, Japan

corresponding author (N. Kogo) email: naoki.kogo@gmail.com

Number of pages: 38
Number of Figures: 10
Number of Tables: 1
Number of words: abstract (150), introduction (648), discussion (1667)

Conflict of interest: none

Acknowledgements

We would like to thank Dr. Ginamaria Maccaferri (Northwestern University, Chicago, USA) for supporting the project during the time of piloting, Dr. Andreas Burkhalter (Washington University, St. Louis, USA) for providing detailed information of the anatomy of mouse visual cortex, Dr. Yoshikazu Isomura (Tamagawa University, Machida, Japan) for supporting to conduct the project and the anatomical analysis at Brain Science Institute, Dr. Nael Nadif Kasri and Dr. Dirk Schubert (RadboudUMC, Nijmegen, The Netherlands) for supporting to run the experiments at their laboratory. Naoki Kogo was supported by a post-doctoral fellowship of Fonds voor Wetenschappelijk Onderzoek (FWO-Flanders post-doc grant 12L5115N, University of Leuven, 2014~2017) and a European Fellowship from Marie Curie Actions (794273, Radboud University,

2018~current). TN was supported by the EPSRC (EP/P006094/1) and European Union (785907). RvW was supported by grants by NWO-TTW (NESTOR and INTENSE).

Abstract

Neural competition plays an essential role in active selection processes of noisy and ambiguous input signals and it is assumed to underlie emergent properties of brain functioning such as perceptual organization and decision making. Despite ample theoretical research on neural competition, experimental tools to allow neurophysiological investigation of competing neurons have not been available. We developed a "hybrid" system where real-life neurons and a computer-simulated neural circuit interacted. It enabled us to construct a mutual inhibition circuit between two real life pyramidal neurons. We then asked what dynamics this minimal unit of neural competition exhibits and compared them to the known behavioral-level dynamics of neural competition. We found that the pair of neurons shows bi-stability when activated simultaneously by current injections. The addition of modelled synaptic noise and changes in the activation strength showed that the dynamics of the circuit are strikingly similar to the known properties of bi-stable visual perception: The distribution of dominance durations showed a right-skewed shape, and the changes of the activation strengths caused changes in dominance, dominance durations, and reversal rates as stated in the well-known empirical laws of bi-stable perception known as Levelt's propositions.

Significance Statement

Visual perception emerges as the result of neural systems actively organizing visual signals that involves selection processes of competing neurons. While the neural competition, realized by a "mutual inhibition" circuit has been examined in many theoretical studies, its properties have not been investigated in real

neurons. We have developed a “hybrid” system where two real-life pyramidal neurons in a mouse brain slice interact through a computer simulated mutual inhibition circuit. We found that simultaneous activation of the neurons leads to bi-stable activity. We investigated the effect of noise and the effect of changes in the activation strength on the dynamics. We observed that the pair of neurons exhibit dynamics strikingly similar to the known properties of bi-stable visual perception.

Introduction

Visual perception is an emergent property resulting from an active organization of input signals by the brain while being subjected to the underrepresented, noisy and ambiguous signals received by the eyes. In other words, the brain makes selections among neural signals representing the conflicting signals that are competing with each other. A well-known perceptual phenomenon representing signal competition and selection processes is "bi-stable perception" that occurs when visual signals support two likely perceptual interpretations. Signals that support one of the percepts are selected coherently at any given time and one percept becomes dominant. The input signals are eventually re-organized to establish the alternative percept, leading to reversals between the two percepts every few seconds (Leopold and Logothetis, 1999). This repetitive perceptual re-organization in bi-stable perception provides information about how visual signals are processed, organized, and eventually lead to conscious perception. The abundant literature on bi-stable perception is an important resource of information to investigate underlying neural mechanisms.

Neural competition is often modelled by "mutual inhibition" between neurons. A possible neural circuit is shown in Figure 1a in which each pyramidal neuron (PN1 or PN2) activates a partner inhibitory neuron (IN1 and IN2, respectively) which, in turn, projects an inhibitory synapse to the competing pyramidal neuron, forming disynaptic inhibitory connections in both directions.

It has been suggested that the conflicting signals for local features such as orientation (Sillito, 1975; Bonds, 1989), motion direction (Mikami et al., 1986; Snowden et al., 1991), and edge assignment (Zhou et al., 2000; Kogo and van Ee, 2015) compete with each other through such mutual inhibition circuits. This

circuit has been implemented in computer models to explain bi-stable perception (Matsuoka, 1984; Mueller, 1990; Wilson, 1999; Wilson et al., 2000; Laing and Chow, 2002; Lankheet, 2006; Noest et al., 2007; Shpiro et al., 2009), object recognition (Masquelier et al., 2009), decision making (Heuer, 1987; Usher and McClelland, 2001; Machens et al., 2005), and place cell field generation (Mark et al., 2017). It has also been suggested that these circuits underlie mechanisms such as larger scale neural interactions and feedback systems (Lee et al., 1999; Beck and Kastner, 2005; Wang et al., 2013) that establish a globally coherent percept. Moreover, disynaptic inhibitory connections between pyramidal neurons are found in various layers and areas of neocortex (Kapfer et al., 2007; Ren et al., 2007; Silberberg and Markram, 2007; Berger et al., 2009) and hippocampus (Miles, 1990). It is hence possible that mutual inhibition serves as a canonical element of signal processing circuits in the brain. (Note, however, that there have been alternative models for bi-stability and decision making that implemented neural mechanisms different from mutual inhibition (Said and Heeger, 2013; Hayden and Moreno-Bote, 2018).)

Despite the numerous theoretical models implementing mutual inhibition circuits, experimental tools are missing that allow thorough neurophysiological analysis of competing cortical neurons at the system-wide level, due to the limitations of current technology. However, with the approach introduced in this paper, it is possible to construct a minimal unit of neural competition in real-life. By investigating the neural dynamics of the minimal unit, considering it as a building block of the whole system, and comparing its dynamics to the ones of

the whole system, it may be possible to deduce how neural elements are integrated into a whole system such that known behavioral properties emerge.

We established a technique where a model mutual inhibition circuit is implemented between a pair of two real-life pyramidal neurons in brain slice preparations of mouse primary visual cortex (Figure 1). The two neurons are patch clamped and connected with each other via a computer model that allows them to interact in real time. This hybrid system has the advantage of keeping all physiological properties of the real pyramidal neurons intact, while providing full control over the computer simulated connections between them. Using this hybrid system, we succeeded to evoke bi-stable activity in the pyramidal neurons. We investigated the dynamics of the bi-stable activity and compared them with the known dynamics of bi-stable visual perception, namely the effects of noise and the effect of changing stimulus input intensity.

Materials and Methods

Experiments were performed at the Brain Science Institute (Tamagawa University, Japan), and the Donders Institute for Brain, Cognition and Behavior, (Radboud University, The Netherlands). The experimental animal procedures were approved by the Animal Research Ethics Committee of Tamagawa University (animal experiment protocol H29/08) and the Animal Ethics Committee of the Radboud University Nijmegen, under DEC application number 2018-0016 (Nijmegen, the Netherlands). The procedures are in accordance with the Guidelines for Animal Experimentation in Neuroscience (Japan Neuroscience Society) and the Dutch legislation.

EXPERIMENTAL DESIGN

Brain slice preparation

Brain slices were prepared from the occipital part of the mouse brain that includes the visual cortex (strain C57BI6/J, age p12 to p24, both sex). Mice were anesthetized deeply using isoflurane in an induction chamber. Following deep anesthesia, mice were quickly decapitated and the brain was removed from the skull in a small container with chilled "cutting solution". For this process, the solution of either one of the following compositions was used (in mM): 125 NaCl, 25 NaHCO3, 2.5 KCl, 1.25 NaH2PO4, 1 $CaCl_2$, 2 $MgCl_2$, 25 D-glucose, or 75 sucrose, 87 NaCl, 25 $NaHCO_3$, 2.5 KCl, 1.25 NaH_2PO_4, 0.5 $CaCl_2$, 7 $MgCl_2$, 25 D-glucose, both saturated with 95% O_2, 5% CO_2. Then, the brain tissue was glued on to the cutting stage of a vibratome (VT1000S, Leica, Germany, or Microm HM 650V, Thermo Scientific, USA), submerged in the cutting solution above. Coronal or angled-coronal (Dong et al., 2004) sections of 300~400μm thickness were cut and stored in an incubation chamber in 32~34°C for at least 30 min, and then stored at room temperature until use.

Double whole-cell recordings

Slices were transferred to a recording chamber on a microscope stage and were superfused with artificial cerebrospinal fluid, ACSF, maintained at a constant temperature (32~34°C). ACSF had the following composition (in mM): 125 NaCl, 25 $NaHCO_3$, 2.5 KCl, 1.25 NaH_2PO_4, 2 $CaCl_2$, 1 $MgCl_2$, 25 D-glucose, saturated with 95% O_2, 5% CO_2. The location of V1 was identified under the microscope (Olympus, Japan) equipped with DIC-IR (differential interference contrast – infrared). Layers of visual cortex were identified and the point where layer 5

starts thickening, going from medial to lateral, was used as a landmark of the border between V1 and LM (lateromedial area, Wang and Burkhalter, 2007, equivalent to V2, Figure 1c). All recordings were made from the region medial from the landmark. Under high magnification with x40 objective, pyramidal neurons in layer 2/3 were identified by their stereotypical morphology. In some cases, the recorded neurons were filled with biocytin and post-experimental process indicated that, in all cases, they were pyramidal neurons in layer 2/3 (see below). Two neurons separated by at least 150μm distance were selected to reduce the probability of choosing connected pairs. Furthermore, experimental protocols were performed to check for monosynaptic (paired-pulse injection at 10Hz to one of the neurons to evoke action potentials) and disynaptic connections (Kapfer et al., 2007; Silberberg and Markram, 2007) (100Hz 11 pulses injection to one of the neurons to evoke a train of action potentials). None of the pairs reported in this paper were connected.

Pipettes for patch clamp recordings were pulled from borosilicate thin glass capillaries (TW150-4, WPI, USA) and filled with a filtered intracellular solution with the following composition (mM). 130 K-gluconate, 10 KCl, 4 ATP-Mg, 0.3 Na-GTP, 10 HEPES, 10 phosphocreatine. For phosphocreatine, either 10mM Na_2-phosphocreatine or a mixture of 5mM Na_2-phosphocreatine and 5mM tris-phosphocreatine was used. The osmolarity of the solution was adjusted to 290~300Osm by either Osmotron-5 (Orion Riken Co., Japan) or Semi-Micro Osmometer K-7400 (Knauer, Germany) and the pH was adjusted to 7.2. The final resistance of the pipettes was 7~9MΩ. In some cases, biocytin was added to the pipette solution (2.5~5mg/ml) to visualize the recorded neurons post-experimentally. Recordings were carried out using either two Axopatch 200B

amplifiers or a Multiclamp 700 amplifier (both Molecular Devices, Sunnyvale, CA, USA). Data were lowpass filtered at 10kHz and were digitized at 20 kHz using a Digidata A/D board model 1440A. Data were captured using the Clampex program suite (Molecular Devices, USA). Series resistances were constantly monitored by injecting a −100pA pulse in current-clamp configuration. Series resistances were balanced via a bridge circuit.

Cell identification

To visualize the pyramidal neuron pairs that were recorded, they were filled with biocytin by diffusion (N=9). After the recording (approximately 30 to 60 minutes), the slices were kept in 4% paraformaldehyde in phosphate buffer solution, PBS, (0.1 M, pH 7.2) and were kept at 4˚C. After washing the tissue with PBS, it was quenched with 1% H_2O_2 in 10% methanol and 90 % PBS for 5 minutes. The tissue was washed with PBS and permeabilized with 2% Triton X-100 in PBS for 1 hour and then put in ABC solution (ABC Elite Kit, Vector, USA) overnight at 4˚C. After washing the tissue with PBS and then with Tris buffer (0.05M), it was processed with DAB solution (0.5g/l in 0.05M Tris buffer) and 1%H_2O_2 was added to enhance the reaction. After verifying the visualization of neurons, the tissue was washed by PBS and then mounted to glass slides with a mounting medium (Aquamount, Vector, USA).

Dynamic clamp

A modified version of the dynamic clamp system StdpC (spike timing dependent plasticity clamp, Nowotny et al., 2006; Kemenes et al., 2011) was used to establish the connections between recorded neurons and model neurons with

model synapses. The communication between the amplifier and StdpC was mediated by a National Instruments A/D board, model PCIe-6321. Dynamic clamp is a method whereby a modelled conductance, e.g. a synaptic or ionic conductance, is computed based on the measured membrane potential of a neuron, then injected into that neuron in real time with a patch clamp electrode. Unlike other dynamic clamp systems which operate at fixed frequencies, StdpC does not require a real-time operating system, relying instead on precise measurement of the time elapsed in each measure-compute-inject cycle to perform the numerical integration of its models.

Besides numerous improvements to the software interface, the following major additions were made to the previous version of StdpC (Nowotny et al., 2006). A passive membrane model was added, which can be augmented with models of ionic and synaptic conductances to form completely synthetic neuron models. To stabilize numerical integration of such models at StdpC's unpredictable and varying sampling frequency, the clamp cycle was upgraded from explicit Euler to a Runge-Kutta integration scheme of order 4/5. A number of performance enhancements were made to ensure high-frequency, and thus high-fidelity, updates to the injected current. A delay mechanism was added to the synapse models, allowing the simulation of conduction and synaptic delays. Finally, a model of synaptic background noise was added, reproducing the synaptic bombardment we would expect to see in vivo with statistically equivalent, randomly generated inhibitory and excitatory currents, as described in the section on noise below. The upgraded version of StdpC (StdpC version 6.1) is available at github.com (github.com/CompEphys-team/stdpc, DOI 10.5281/zenodo.3492203).

A custom-made summing circuit was used to combine the command signal from StdpC and the one from Clampex software, and the combined command signal was fed to the amplifier.

Hodgkin-Huxley models of ionic channels (conventional sodium, delayed rectifier potassium, and Kv3 potassium channels) were given to the model inhibitory neuron (membrane capacitance 0.2115nF, leak conductance 63.462nS, equilibrium potential for the leak conductance -70mV (Pospischil et al., 2008)). A Kv3 channel was added to simulate fast spiking inhibitory neurons(Lien and Jonas, 2003). The models are based on an "α/β formalism" as follows (see github.com/CompEphys-team/stdpc/tree/master/manual).

$$I = g_{max} m^p h^q (V - V_{rev})$$

$$\frac{dm}{dt} = \alpha_m (1 - m) - \beta_m m$$

$$\alpha_m = k_{\alpha,m} F_{\alpha,m} \left(\frac{V - V_{\alpha,m}}{s_{\alpha,m}} \right)$$

$$\beta_m = k_{\beta,m} F_{\beta,m} \left(\frac{V - V_{\beta,m}}{s_{\beta,m}} \right)$$

(and analogous for h).

Here, m and h are activation and inactivation variables. g_{max} is the maximum conductance of the ion channel and V_{rev} is the reversal potential of the ion. The form of the function F is either one of the three below.

$$F_1(x) = \frac{x}{\exp(x) - 1}$$

$$F_2(x) = \exp(x)$$

$$F_3(x) = \frac{1}{1 + \exp(x)}$$

For the potassium channels, the formalisms are the same, except that no inactivation components are included. The form of the function F and the parameters for α and β for the individual components are as summarized in Table 1 (top). These parameter values were taken from Pospischil *et al.* (Pospischil et al., 2008) for basic membrane properties, from Hodgkin & Huxley(Hodgkin and Huxley, 1952) for sodium and delayed rectifier potassium channels and from Lien & Jonas (Lien and Jonas, 2003 p.3) for KV3 channel.

Conductance of excitatory and inhibitory synaptic events were modeled using the ChemSyn model in StdpC, following the equations and parameters described below.

$$I = g_{syn} S(t)(V_{syn} - V_{post}(t))$$

$$\tau_{syn} \frac{dS(t)}{dt} = \frac{S_\infty(V_{pre}(t)) - S(t)}{1 - S_\infty(V_{pre}(t))}$$

$$S_\infty(V_{pre}(t)) = \begin{cases} \tanh\left(\frac{V_{pre}(t) - V_{TH}}{V_{slope}}\right) & if\ V_{pre}(t) > V_{TH} \\ 0 & otherwise \end{cases}$$

Parameters for excitatory and inhibitory synapses are shown in Table 1 (middle). g_{syn} for EPSP was selected so that it evokes an action potential in mINs (Figure 2), and g_{syn} and τ_{syn} for IPSP were selected to ensure strong enough suppression of target PN. The synaptic delay was set to 1ms in all cases, and no synaptic plasticity was included in the model.

Disynaptic mutual inhibition connections

Establishment of a mutual inhibition circuit was verified as follows. Injection of a brief (1ms) depolarization current (1500~2000pA) to one of the pairs of pyramidal neurons evoked an action potential (red and blue triangles in Figure 2a), which triggered an excitatory synaptic conductance in the model inhibitory neuron. This synaptic event evoked an EPSP in the inhibitory neuron. As shown in Figure 2a, when g_{syn} was set to 10nS or higher, the EPSP evoked an action potential (red and blue disks). This action potential in the inhibitory neuron triggered an inhibitory synaptic conductance, which was fed to the postsynaptic pyramidal neuron as an injected IPSC via the amplifier, giving rise to a corresponding IPSP (blue and red asterisks). Figure 2a shows that an action potential was first evoked in the pyramidal neuron 1 (PN1) and the pyramidal neuron 2 (PN2) received an IPSP. Later, an action potential was evoked in PN2 that resulted in an IPSP given to PN1, illustrating that the mutual inhibition circuit was established between the two pyramidal neurons by this system. As shown in Figure 2b, the inhibitory neurons show trains of action potentials corresponding to the action potentials of presynaptic pyramidal neurons during bi-stable activity.

Bi-stable activity

Bi-stable activity in a pair of pyramidal neurons is evoked by the following protocol. First, before the dynamic clamp mediated model circuit is switched on, depolarization currents that evoke action potentials at approximately 10 Hz in the two neurons are determined separately. Next, the model circuit is switched

on to activate the mutual inhibitory connection, and the depolarization currents as determined above are injected. In most cases, this already produces bi-stable activity in the pair (unless one of the neurons is 100% dominant). However, every neuron has different firing patterns, different degrees of responses to given synaptic inputs, and different sizes of action potentials (which influence the strength of postsynaptic events). As a result, the bi-stable activity often does not show equal dominance between the two neurons even though the firing rates are equivalent between them. Therefore, in the case that it is necessary to find the current pair where the dominance of the two neurons are approximately equal (50% dominance point), the currents are further adjusted by either increasing the current in the weaker neuron or decreasing the current in the stronger neuron.

Dominance, dominance durations, and reversal rates were calculated using custom Matlab (MathWorks, USA) scripts. Unlike behavioral studies, in which a dominant percept is indicated as a continuous signal (by button press), the dominance of a neuron is signaled by sustained repetitive firing of action potentials. Hence, we defined the "dominance duration" of a neuron as follows (illustrated in Figure 3). First, a continuous firing of action potentials in one neuron until an action potential occurs in the other neuron is considered as a tentative dominance duration of the neuron (Figure 3b). Hence, at this stage, the dominance durations of the two neurons are mutually exclusive. Note that there are short dominance durations (blue asterisks for PN2 and red asterisk for PN1). There are also a series of alternations of short dominance durations between the two neurons (green asterisks). Next, dominance durations shorter than 250ms are eliminated (Figure 3c). This process results in short lags between the

dominance durations (blue and red asterisks). The occurrence of the short lag is not considered as reversal and, hence, the previous dominance is considered to continue (arrows). These processes result in the final dominance durations without short durations (Figure 3d). Note that there are also the intervals that are not assigned to either of the neurons corresponding to the period marked with green asterisks in Figure 3c. This is because alternating short durations occur between the two neurons during these periods (Figure 3c green asterisks). These periods are assigned as "both active" (Figure 3d bottom). Dominance and reversal rates were computed based on this definition of dominance durations. "Dominance" of a neuron is defined as the ratio of total dominance durations of the neuron (sum of all dominance durations of the neuron) divided by the sum of the total dominance durations of both neurons. A reversal is defined as the dominance switching from one neuron to the other, regardless of the presence or absence of a "both active" phase during the switch. The coefficient of variation of dominance durations was computed according to Pastukhov and Braun (Pastukhov and Braun, 2011).

Special attention was paid to the recording conditions. If the following criterion were not met, the recording was halted: The overshoot of action potential should be higher than 10mV, and changes in the size of the action potential, in series resistance, and in firing rate to a given depolarization current should be less than 15% during data collection.

Analysis of adaptation

Inter-spike intervals and the peaks of action potentials were estimated with custom Matlab scripts. Upon detection of action potentials inter-spike intervals

and the peaks were measured. These values were plotted against time to visualize the progress of adaptation within individual dominance episodes. To pool the data, first, the time from the onset of the dominance cycle to the end of this cycle was normalized by dividing it by the cycle's dominance duration (for the individual cycles of the individual pairs), resulting in the normalized time ranging from 0 to 1. Second, inter-spike intervals and the magnitude of action potential peaks were normalized by the first values of the individual cycles. Third, the normalized values across all pairs were sorted into bins of size 0.01. Finally, the mean and standard deviation of all inter-spike intervals and action potential peaks in a given bin were plotted against the normalized time. As an indicator of the progress of adaptation, inter-spike intervals (normalized by the mean of individual pair) was plotted over time from the onset of each dominance cycle and linear regression was applied to the plot (Figure 4). This resulted in slope values that indicated the change of inter-spike intervals. To pool the data, the dominance durations of individual pairs were normalized by their mean values and the slopes, normalized by the mean values of individual neurons, were plotted over the normalized duration.

Effect of noise

To investigate the effect of noise on the dynamics of bi-stable activity, synaptic background activity was simulated according to the model by Destexhe *et al.* (Destexhe et al., 2001). In their simulation, random walk-like fluctuations of membrane conductance were modeled by applying the Ornstein-Uhlenbeck model of Brownian motion (Uhlenbeck and Ornstein, 1930). Their formalism of synaptic noise was implemented in the StdpC dynamic clamp system. The

evolution of the simulated synaptic noise depends on the noise time constant τ, which controls noise color, as well as the mean g_{mean} and standard deviation SD_g of the noise, and is modeled as follows:

$$I = g(t)(V_{rev} - V)$$

$$g(t + \Delta t) = g_{mean} + (g(t) - g_{mean})\, e^{-\frac{\Delta t}{\tau}} + Ar$$

$$A = \sqrt{\frac{D\tau}{2}\left(1 - e^{-\frac{2\Delta t}{\tau}}\right)}$$

Here, r is a pseudo-random number drawn from a normal distribution with mean 0 and standard deviation 1, and the noise diffusion coefficient D is related to the noise standard deviation as follows:

$$D = \frac{2\, SD^2 g}{\tau}$$

Excitatory and inhibitory synaptic noise are modeled separately. The level of noise is expressed as the standard deviation SD_g of the synaptic conductance and systematically manipulated, whereas the average conductance g_{mean}, which functions as a constant current offset, remained unchanged. The amount of noise given to mINs was larger than that given to PNs because PNs already have intrinsic synaptic noise (Figure 7a) from their presynaptic neurons within the brain slice. The standard parameter set (used as default unless mentioned otherwise) for the noise is shown in Table 1 (bottom).

In the experiments for the effect of noise level and the effect of activation level (below), the length of each trial was 200 sec with 193.5 sec long depolarization current.

Effect of short-term plasticity

It has been reported that there are diverse and cell-type specific short-term plasticity effects in neocortex and hippocampus (see Markram et al., 2004; Silberberg et al., 2005; Tremblay et al., 2016; Pelkey et al., 2017 for review). To explore its effect on bi-stable activity, short-term depression was implemented in the model synaptic conductance in StdpC by introducing a depression factor, *h*, defined as follows.

$$I = g_{syn}S(t)h(t)(V_{syn} - V_{post}(t))$$

$$\tau_h \frac{dh(t)}{dt} = h_\infty\big(V_{pre}(t)\big) - h(t)$$

$$h_\infty\big(V_{pre}\big) = \frac{1}{1 + exp\left(\frac{V_{pre} - V_{Thresh,h}}{V_{Slope,h}}\right)}$$

$$\tau_h\big(V_{pre}\big) = \tau_0 - \frac{\tau_{Ampl}}{1 + exp\left(\frac{V_{pre} - V_{Thresh,\tau}}{V_{Slope,\tau}}\right)}$$

STD was modelled in both excitatory synapses from pyramidal neurons to fast spiking neurons and to inhibitory synapses from fast spiking neurons to pyramidal neurons with the following parameters.

$V_{Thresh,h} = -20mV$, $V_{Slope,h} = 2mV$, $\tau_0 = 2.5ms$, $\tau_{Ampl} = -0.8$, $V_{Thresh,\tau} = -20mV, V_{Slope,\tau} = 2mV$

Depression of PSPs was verified by generating a train of artificial spikes within StdpC by means of a Spike Generator (SG), connected by model synapses to a model neuron where EPSPs were evoked (Figure 11A). The effect of STD was observed with two synaptic strengths (g_{syn}=20nS and g_{syn}=50nS) applied to all synapses in the circuit, chosen to demonstrate both successful mutual inhibition (g_{syn}=50nS), and failed mutual inhibition (g_{syn}=20nS) due to insufficient activation of the inhibitory neurons.

Paradigms equivalent to Levelt's experiments

For our experiments associated with the classic behavioral experiments of Levelt (Levelt, 1965, see also Brascamp et al., 2006, 2015; Moreno-Bote et al., 2010 for generalized Levelt's propositions covering the full-range of stimulus intensities) we systematically varied the strength of the sustained depolarization current into one, or both, of the pyramidal neurons. Concerning the generalized Levelt's proposition I to III, the two currents were set as follows. First, the currents were set to evoke 10Hz firing rate in the individual neurons (without mutual connections). Next, the modelled mutual inhibition circuit was activated while maintaining the static current injections. Then, only one of the two currents (randomly selected) was altered. The change of the current was made by steps of 10 or 20pA.

In the analyses, the current that would evoke 50% dominance, called $I_{50\%}$, was estimated by linear regression of dominance over the changing current. The change of the current is reported with reference to this control current value, defined as follows.

$$\Delta I_{50\% norm} = \frac{I - I_{50\%}}{I_{50\%}}$$

Hence, in the plots in Figure 8c to 8h, the right side from x=0 indicates that the neuron that received the changing current was more dominant (stronger) than the other neuron and the left side indicates the former being weaker than the latter. Before pooling the data (N=46) for average durations, average dominance durations of individual trials were computed and were divided by the maximum

455 average duration within individual neuron. To pool the data for the reversal rate,
456 data were normalized by the maximum reversal rate of the individual pair.
457 Concerning the generalized Levelt's proposition IV, both currents were modified.
458 First, a current pair that evoked a 10Hz firing rate in the two neurons was found.
459 If necessary, the current was adjusted until the current pair evoked
460 approximately 50% dominance. This current pair was considered as a control
461 and is called I_{10Hz} (it is called as such for convenience although the current pair
462 did not always evoke 10Hz firing). Next, in one of the two neurons, the current
463 was changed with 10 or 20pA steps and the current for the other neuron was
464 changed proportionally. To pool the data, the change of the current is reported
465 with reference to I_{10Hz}, defined as follows.

$$\Delta I_{10Hznorm} = \frac{I - I_{10Hz}}{I_{10Hz}}$$

466 To pool the data for the reversal rate (N=32), data were normalized by the
467 reversal rate of the individual pair when the control current pair was used.
468 To make the bar plots of the pooled data (Figure 8f to h, right, Figure 10c
469 bottom), the ΔI was binned and the values in the individual bins were averaged.
470 The order of trials with different current pairs was pseudo-randomly chosen.
471

472 **STATISTICAL ANALYSIS**

473 For statistical analysis, repeated measures analysis of variance (ANOVA) was
474 applied using SPSS Statistics (IBM, USA). Pairs with the standard noise
475 parameter set for the experiment of noise (N=15), pairs with injected current of
476 $I_{50\%}$ in Levelt I to III paradigms (N=46), and pairs with injected current of I_{10Hz} in
477 Levelt IV paradigm (N=32) are collectively called a "control pair" and statistical

478 analyses were performed on these 93 pairs to report basic properties of bi-
479 stability and adaptation. Error bars in the plots are +/- SEM.
480 All data and Matlab codes for data analyses are published at Radboud University
481 data repository site with URL as below.
482 https://data.donders.ru.nl/collections/di/dcn/DAC_626810_0008_424?93
483

484 **Results**

485 Double patch clamp recordings were performed from visually identified
486 pyramidal neurons in layer 2/3 of mouse primary visual cortex (Figure 1c). In
487 total, 93 pairs of pyramidal neurons from 32 mice were recorded. By using
488 biocytin-filled patch pipettes, some pyramidal neuron pairs were labeled and
489 visualized after the experiments (N=9). In all cases, the stereotypical morphology
490 of pyramidal neurons (with a short apical dendrite and thin multiple oblique
491 dendrites) was identified, located in layer 2/3 of V1 (Figure 1d).
492

493 **Bi-stable activity**

494 Mutual inhibitory connections between each pair of pyramidal neurons were
495 constructed by the StdpC dynamic clamp system (see Materials and Methods for
496 details). When continuous depolarization currents were injected into PN1 and
497 PN2 simultaneously, bi-stable activity with alternating dominance between the
498 two pyramidal neurons was evoked as shown in Figure 5a. Figure 5b shows the
499 details of the onset of the response to the current injection on a shorter time
500 scale. Both neurons started to depolarize at the onset but PN2 reached the action
501 potential threshold before PN1 and, hence, PN1 received the evoked IPSP before
502 succeeding to generate an action potential. Thereafter, PN2 showed sustained

503 firing of action potentials and it achieved initial dominance. Note, that an
504 increase of inter-spike intervals in the dominant neuron is visible. Also note that
505 there is a ramp-like slow depolarization of the suppressed neuron (Figure 5a).
506 The former is a sign of neural adaptation while the latter indicates both the
507 recovery of the neuron from adaptation as well as the recovery of the membrane
508 potential from IPSPs due to the gradual increase of the inter-spike intervals.
509 Figure 5c shows data from when the reversal of dominance occurred. With the
510 continuous increase of inter-spike interval in PN2, PN1 recovered more and
511 more from the received barrage of IPSPs. The inter-spike interval of PN2
512 eventually became long enough such that the membrane potential of PN1
513 reached the action potential threshold before PN2 could generate an action
514 potential. Consequently, PN2 received an IPSP evoked by the first action
515 potential of PN1. From then on, PN1 became dominant and PN2 became
516 suppressed.
517
518 **Adaptation and dominance durations**
519 To investigate the role of adaptation in the mutual inhibition competition
520 process, we analyzed neurophysiological properties that reflect adaptation:
521 inter-spike intervals and peaks of action potentials are plotted in Figure 6a, b,
522 respectively, for the example bi-stable activity shown in Figure 5a. Normalized
523 values are pooled for the "control pairs" (N=93, see Materials and Methods for
524 the definition of the "control pairs") and plotted over normalized dominance
525 durations in Figure 6c, d, for inter-spike intervals and action potential peaks,
526 respectively. The results indicate monotonic changes (increase of inter-spike
527 intervals and decrease of action potential peaks over time) while a neuron is

528 dominant. Furthermore, there are clear correlations between the dominance
529 durations and the changes of the inter-spike intervals. We applied a linear
530 regression to inter-spike intervals as a function of time in the dominance
531 duration (see Figure 4). The slope indicates how quickly the adaptation
532 progresses. As shown in Figure 6e (for the example shown in Figure 5a) and
533 Figure 6f (for the pooled data of the control pairs), the slopes and the dominance
534 durations were inversely correlated (repeated measures ANOVA for the pooled
535 data $F(3,15)=19.518, p<0.0001$). Hence, when adaptation progresses quickly, the
536 dominance duration is bound to be shorter, indicating a role for adaptation in
537 dominance reversals.
538
539 **Effect of noise**
540 Because of the stochasticity of dominance durations (Brascamp et al., 2006
541 p.2006; Kim et al., 2006; Moreno-Bote et al., 2007; Huguet et al., 2014; Pisarchik
542 et al., 2014) it has been argued that noise plays an important role for the reversal
543 in bi-stable perception. To investigate the role of noise on the dynamics of bi-
544 stability, we implemented an algorithm in the dynamic clamp system to
545 introduce simulated noise of the synaptic conductance (Destexhe et al., 2001;
546 Delgado et al., 2010). The noise was given to both PNs and mINs in the form of
547 random fluctuations of excitatory and inhibitory synaptic conductance (see
548 Materials and Methods for details). Figure 7a shows the baseline membrane
549 potential of a pyramidal neuron and Figure 7b shows the result of adding the
550 modeled synaptic noise to it (all at -60mV). Next, the level of noise was changed
551 systematically while the two pyramidal neurons were exhibiting bi-stable
552 activity as shown in Figure 7c (the parameter sets for different noise level are

553 shown in the table in Figure 7d). The results indicate that increased noise caused
554 an increase of the reversal rate (*F(19,171)=50.868, p<0.0001*). The pooled data
555 from 15 pairs of pyramidal neurons are shown in Figure 7d.
556
557 It is known that, in brain slice preparations, the amount of synaptic noise in
558 individual neurons is much less than what is observed in intact brain
559 preparations due to the cutoff of axons and lesser spontaneous activity in slice
560 preparations (Destexhe et al., 2001). Therefore, to reproduce the intact brain
561 environment, we use a parameter set of modelled excitatory and inhibitory
562 synaptic noise which will be called the "standard noise parameter set" (asterisk
563 in Figure 7c and 7d table) from here on. For the rest of the experiments, the
564 standard noise parameter set was used. The histogram of dominance durations
565 of a 600 sec recording of bi-stable activity with the standard parameter set is
566 shown in Figure 7e. It shows a skewed distribution as stereotypically observed
567 in bi-stable perception. The average of dominance durations and reversal rates
568 of the 15 pairs with the standard noise parameter set were 7.7±5.6sec and
569 12.0±10.5min^{-1}, respectively. These values for the control pairs (N=93) were
570 8.2±7.8sec and 11.5±10.8min^{-1}, respectively. The coefficient of variation of
571 dominance durations of the control pairs was 0.60±0.21.
572
573 **Effect of current intensity ("generalized Levelt paradigms")**
574 A set of widely replicated empirical laws from the perceptual competition
575 literature —known as Levelt's propositions— describes the relationship
576 between the strengths of two competing stimuli and the dynamics of their bi-
577 stable perception (Levelt, 1965) in terms of dominance, dominance duration, and

reversal rate. Furthermore, the paper by Brascamp and Klink (Brascamp et al., 2015) and Moreno-Bote et al. (Moreno-Bote et al., 2010) reported a generally accepted updated version of Levelt's propositions so that the description of bi-stable dynamics covers the full range of stimulus strengths (Levelt's original propositions were based on the range of stimulation where the stimulus strength of one of the two input signals increased, and hence, the effect of decreasing the strength was not included). To compare the dynamics of the pairs of mutually inhibited pyramidal neurons to the generalized Levelt's propositions, we injected sustained depolarization currents and systematically varied (increased and decreased) the strength of the current into one, or both, of the pyramidal neurons (Figure 8a).

To examine the first three generalized propositions of Levelt, the current injected into one of the two neurons was varied while the current injected into the other neuron was kept constant (Figure 8b). In total, 46 pairs were recorded with this paradigm. To pool the data, first, the current that would evoke 50% dominance (the total period that one neuron is dominant over the other is equal for both neurons) was estimated ($I_{50\%}$) by linear regression of dominance over the changed current. The change of the current is reported with reference to this control current value (i.e., 0 in abscissa indicates the current pair that would evoke 50% dominance). Hence, in the plots shown in Figure 8c to 8h, the neurons with the changing injected current is more dominant ("stronger") on the right side of the plot from 0, while on the left side, they are less dominant ("weaker").

602 We first tested the generalized Levelt's proposition I: Increasing stimulus
603 strength for one of the competing stimuli will increase the perceptual dominance
604 of that stimulus. Figure 8c depicts the change of the dominance ratios of the two
605 pyramidal neurons over injected current (with reference to $I_{50\%}$ of PN1) for the
606 example shown in Figure 8b. There is a clear trend of increase of dominance of
607 PN1 whose current was increased (red) and of decrease of dominance of PN2
608 whose current was kept constant (blue). Figure 8f shows pooled data (N=46) for
609 the dominance ratio, replicating that there is an increasing dominance of the
610 neurons whose currents were increased (red, *F(6,24)=15.558, p<0.0001*), and
611 decreasing dominance for their counterparts whose currents were kept constant
612 (blue, *F(6,24)=15.558, p<0.0001*)). This is in line with the generalized Levelt's
613 proposition I.
614
615 Levelt's proposition II states: Increasing the difference in stimulus strength
616 between the two competing stimuli will primarily act to increase the average
617 perceptual dominance duration of the stronger stimulus. Furthermore, the
618 generalized Levelt's proposition II states that the change of stimulus intensity of
619 the non-dominant input is less effective. This means that when the stimulus
620 intensity changes from non-dominant range to dominant range, the effect of the
621 change to average dominant durations is weak in the non-dominant range and
622 strong in the dominant range. In Figure 8d the change of the average dominance
623 durations is plotted over the changing current for the example shown in Figure
624 8b. PN1 shows weak changes of the dominance durations on the left half of the
625 plot where PN1 is weaker than PN2 (see Discussion). It shows, however, a steep
626 increase on the right half of the plot where it is stronger than PN2, and vice versa

for the other neuron. Hence, in general, the dominant neuron shows a steep increase of the dominance durations with current values deviating further away from $I_{50\%}$. This trend can be seen in Figure 8g with pooled data for the neurons whose currents were increased (red, $F(6,24)=4.371,\ p<0.01$)) and for their counter parts whose currents were kept constant (blue, $F(6,24)=7.396,\ p<0.0001$). This is in line with the generalized Levelt's proposition II.

According to the generalized Levelt's proposition III: Increasing the difference in stimulus strength between the two competing stimuli will reduce the perceptual alternation rate. Figure 8e plots the number of reversals for the example shown in Figure 8b. The pair showed a higher number of reversals for a current close to $I_{50\%}$. Deviating further from $I_{50\%}$ in either direction, the values decreased, in line with the generalized Levelt's proposition III. However, the pooled data (Figure 8h) show that the response is not symmetric. In fact, some pairs showed an increase of the reversal rate when a neuron is dominant (Figure 9 bottom), in contrast to the example pair of Figure 8b (and Figure 9 top). Thus, the pyramidal neuron pairs did not always follow the generalized Levelt's proposition III. Due to the increase in the left half, repeated measures ANOVA indicated a significant effect ($F(6,24)=2.663,\ p<0.05$).

To examine the generalized fourth proposition of Levelt, the currents injected into both neurons were varied. In total, 32 pairs were recorded with this paradigm. To pool the data, the change of the current is reported with reference to the current that would evoke approximately 10Hz (I_{10Hz}, see Materials and Methods).

Proposition IV states: Increasing stimulus strength of both competing stimuli will generally increase the perceptual alternation rate. In addition, the generalized proposition IV (Brascamp et al., 2015) noted that this effect may reverse at near-threshold stimulus strengths (i.e. the lower range of stimulation intensity). Figure 10a shows an example of the effect of increasing the injected currents into both neurons. In Figure 10b, the number of reversals of this example are plotted over the injected current. Figure 10c shows pooled data indicating increasing reversal rates (*F(6,30)=4.051, p<0.01*). In addition, there is a small decrease of the reversal rate at the lower range of the stimulation. These results are in line with the generalized Levelt's proposition IV.

Effect of short-term plasticity

To explore the role of synaptic plasticity in neural competition and bi-stable activity, we implemented short-term depression (STD) in the modelled excitatory and inhibitory synapses. Figure 11a shows the depression of EPSPs evoked by a train of modelled presynaptic spikes (generated by Spike Generator, SG, at 40Hz). Figure 11b shows the results from a circuit with disynaptic inhibitory connections established between SG, model inhibitory neurons (mINs) and real-life pyramidal neurons (PNs) as illustrated in the schematic. The membrane potentials of the PNs were set to -60mV to make IPSPs visible. Three different conditions were tested: "without STD", "with STD with strong synaptic inputs" (g_{syn}=50nS), and "with STD with weak synaptic inputs" (g_{syn}=20nS), implemented in both EPSPs and IPSPs. A train of ten spikes was generated at 20Hz in the SG. EPSPs without STD successfully evoked action potentials in INs in response to all ten EPSPs (left column). These action potentials, in turn,

677 evoked long lasting IPSPs in PNs (right column). When STD was implemented,
678 the gradual decrease of EPSP size caused failures of evoking action potentials
679 (marked by black asterisks) in INs. Compared with stronger EPSPs (middle
680 traces), this effect was more pronounced with weaker EPSPs (bottom traces).
681 The effect of implementing STD in PSPs as above on bi-stable activity is shown in
682 Figure 11c. Bi-stable activity without STD is shown in the top traces. With STD
683 with strong PSPs (middle traces), the pair of pyramidal neurons showed bi-
684 stability. However, due to the depression of EPSPs, action potentials in the
685 dominant PN soon failed to evoke action potentials in the connected IN and the
686 reversal of dominance occurred quickly. As a result, the reversal rate became
687 higher than the without STD condition. The ratio of reversal rate, with STD to
688 without STD, was 8.6±4.2 (N=9). In contrast, with STD with weak PSPs (bottom
689 trances), action potentials in PNs failed to evoke action potentials in INs most of
690 the time and neither of the PNs was able to establish dominance in competition.
691 Instead, both PNs showed continuous firing of action potentials without an
692 apparent influence on the competing PNs (N=7).
693
694 **Discussion**
695 We established a mutual inhibition between two real-life neurons mediated by
696 dynamic clamp. This system enabled us to evoke bi-stable activity in pyramidal
697 neurons in visual cortex. We analyzed the dynamics of the bi-stability, a number
698 of physiological properties, and the effects of manipulating the level of
699 background noise and activation level. We compared the dynamics of this bi-
700 stability with the known dynamics of human bi-stable perception. Although our
701 experimental system represents the simplest neural unit of competition and

human behavior represents the highly complex system, we found that the two systems show striking similarities in their dynamics.

The analyses of the physiological properties during bi-stable activity showed signs of adaptation of the dominant neurons. Moreover, the variations of inter-spike intervals and dominance durations were correlated, indicating a causal link between neural adaptation and the reversals in bi-stability. Neural adaptation has only been *assumed* as a key element for bi-stable perception theoretically (Matsuoka, 1984; Mueller, 1990; Wilson, 1999; Wilson et al., 2000; Laing and Chow, 2002; Lankheet, 2006; Noest et al., 2007; Shpiro et al., 2009) or it has been *shown indirectly* in the form of decreased contrast sensitivity (Alais et al., 2010). Our data directly show, in physiological terms, a progression of adaptation during bi-stable activity and its link to the dominance durations.

We investigated the effect of neural noise on the dynamics of bi-stability. The apparent stochasticity in the sequence of reversals and the skewed distribution of dominance durations (Levelt, 1967) in bi-stable perception led to studies on the role of noise (Brascamp et al., 2006; Kim et al., 2006; Moreno-Bote et al., 2007; Huguet et al., 2014; Pisarchik et al., 2014; Baker and Richard, 2019). To investigate the effect of noise in our experimental model, we incorporated a neuro-computational model of synaptic noise into the dynamic clamp. In this way, we were able to insert noise into neurons and systematically changed the level of noise. We found that an increase of noise caused an increase of reversal rate. It is known that the synaptic noise in brain slice preparations is much less than the noise in intact brains (Destexhe et al., 2001) or in human brain tissue (Molnár et al., 2008). Hence, we added noise levels equivalent to the noise level in the intact brain (Destexhe et al., 2001). We found that the histogram of

727 dominance durations was right-skewed as is typically found in bi-stable
728 perception.
729 We showed that when one of the two neurons is dominant, its adaptation
730 progresses and hence the inter-spike interval increases over time. This allows
731 the suppressed neuron to recover from its own adaption and to depolarize more
732 during the ever-increasing inter-spike intervals of the dominant neuron,
733 consequently showing a slowly ramping depolarization. When the membrane
734 potential comes close to the firing threshold, the noise facilitates the membrane
735 potential to go above the threshold, generating action potentials. As a
736 consequence, the dominant neuron now receives IPSPs and a reversal occurs.
737 Hence, our data elucidate the dynamic interplay between adaptation, noise and
738 mutual inhibition in determining the dynamics of bi-stable activity.
739 Our experimental model allowed us to separately manipulate the levels of
740 activation of the competing neurons. Hence, it enabled us to compare the effects
741 of changing activation levels in neurons to the effects of changes in stimulus
742 strength on bi-stable perception, as originally described in Levelt's four
743 propositions (Levelt, 1965). Levelt's propositions I, II and III make predictions
744 about the changes of dominance, the dominance durations, and the reversal rate,
745 respectively, in response to changes of the stimulation strength in one of the two
746 inputs. Levelt's proposition IV concerns the change in the reversal rate while the
747 stimulus strengths of both inputs are changed concurrently. The original
748 propositions were modified later (Brascamp et al., 2006, 2015; Moreno-Bote et
749 al., 2010) to cover the whole range of the stimulus strength (dominant and non-
750 dominant ranges). By running paradigms equivalent to these experiments, we
751 found that both systems show striking similarities in their dynamics.

It is quite intriguing that, although the overall effect of increasing the injected current was the increase of the reversal rate in the paradigm for the generalized Levelt's proposition IV, we observed a small decrease of it in the lower range of the injected currents. A small deviation of the response from the original proposition by Levelt has been reported by several papers (Shpiro et al., 2007; Curtu et al., 2008; Seely and Chow, 2011, see Brascamp et al., 2015). In our experiment, when the injection current was lowered, generation of action potentials by the dominant neuron became sporadic. As a result, the spike interval became longer, giving room to the suppressed neuron to recover from the inhibition and reach the threshold of action potentials. On the one hand, in the higher range of injection currents, the reversal occurred because spike intervals of the dominant neuron gradually increased due to adaptation. On the other hand, in the lower range of injection currents, the reversal occurred because of the lower frequency of evoked action potentials. The latter may be potentially a mechanism underlying the small decrease in the lower range of stimulus reported in bi-stable perception.

One exception where our data did not necessarily match the known dynamics of bi-stable perception was the mixed results for the Levelt III paradigm. In this paradigm, some neuron pairs showed a decrease of reversal rates when the depolarization current either increased or decreased from the control value which is in line with the generalized Levelt's proposition III. However, other pairs showed no significant change or an increase of reversal rate when the current was higher than the control. The mixed results suggest involvement of multiple factors. The reversal rate is determined by the balance between increased dominance durations of the stronger neuron and decreased

dominance durations of the weaker neuron. If the former is more significant, the reversal rate will decrease and if the latter is more significant, it will increase. The increase of the firing rate in the stronger neuron may cause a stronger dominance of the neuron on one hand, and a stronger adaptation of the neuron on the other hand. The latter may prevent the increase of the dominant durations due to the faster decay of the firing rate. Hence, depending on the adaptation properties and the spiking properties of the neurons, the strong activation of the stronger neuron may have caused a decrease of the reversal rate in some cases and an increase in other cases. At systems level, the competition is between populations of neurons rather than single neurons as tested here. Hence, differences in adaptation and spiking properties among the involved neurons may collectively have different impacts on the dynamics of bi-stability. Furthermore, in the human brain, the input signals go through multiple steps of normalization before reaching the mutual inhibition processes. It may be possible that the activation level of neurons in the human visual system is kept within the range where the fast adaptation occurs in a lesser amount. If this is the case, the strong stimulation would cause the decrease of the reversal rate as reported in the generalized Levelt III. Therefore, this result may represent an example where emergent properties of bi-stable perception at the behavioral-level differ from the dynamics found in the minimal neural competition unit we investigated.

Regarding the dominance durations, there are short periods when the neuron that has been suppressed fires only one or two action potentials and then becomes suppressed again. Such short events are not considered as a reversal in our analyses, and the dominance durations are determined by neglecting these

802 events (see Figure 3). Furthermore, there are periods where short events
803 occurred alternatingly between the two neurons with intermingled action
804 potentials from both neurons. In these periods, none of the two neurons are
805 considered to be dominant. These observations may be linked to known
806 observations in bi-stable perception. It has been reported that human subjects
807 experience short reversal events detected in reflexes (optokinetic nystagmus
808 and pupil dilations) but they are too short to be reported by the subjects (Naber
809 et al., 2011). Furthermore, the intermingled firing of action potentials by the two
810 neurons may be related to the period in bi-stable perception where the
811 perception of the subject is either uncertain or a mixture of the two possible
812 percepts ("composite" or "mixed" perception). The short and the mixture events
813 are potentially important because they may elucidate the neural mechanisms
814 underlying the stochastic properties of bi-stability and decision making
815 processes. Hence, this intriguing property of bi-stable neural activity during the
816 transition of the dominances should be investigated further in future.
817 Finally, it is important to consider the diversity of neural properties in neocortex.
818 First, in terms of the location where neural competition relevant to bi-stable
819 perception takes place, it is unknown which layer and which area of visual cortex
820 is involved. It is also possible that the final decision is the result of integrating
821 neural competition at multiple levels. In addition to the issue of location, neurons
822 display a range of firing patterns even within the same area and the same layer.
823 At the onset of activation, for example, an early bursting type pyramidal neuron
824 may have an advantage over a regular-spiking type pyramidal neuron to win the
825 onset dominance. Different adaptation properties influence how the reversal of
826 dominance occurs as well. The differences of these properties are present not

827 only in pyramidal neurons but also in inhibitory neurons, e.g. non-adapting fast
828 spiking neurons or adapting type regular spiking neurons. Furthermore, cell type
829 specific short-term plasticity has been shown. Therefore, it is important to
830 diversify the research on neural competition reported here by applying our
831 approach to neurons from different layers with different firing patterns,
832 adaptation properties, and synaptic properties. How details of the dynamics of
833 bi-stability change depending on these neurophysiological differences remains
834 to be elucidated by future research.
835
836 Concluding, our experimental model provides a platform for investigating the
837 dynamics of a theoretically derived neural circuit in real-life neurons. Our data
838 showed that even the simplest neural competition circuit already reproduces
839 many aspects of dynamics of bi-stable perception in human perception. Our
840 study using the novel approach reported here provides a platform to investigate
841 further how elementary neural competition units are integrated to execute
842 system-level bi-stable dynamics.
843

844 **References**

845 Alais D, Cass J, O'Shea RP, Blake R (2010) Visual sensitivity underlying changes
846 in visual consciousness. Current Biology 20:1362–1367.

847 Baker DH, Richard B (2019) Dynamic properties of internal noise probed by
848 modulating binocular rivalry. PLOS Computational Biology 15:e1007071.

849 Beck DM, Kastner S (2005) Stimulus context modulates competition in human
850 extrastriate cortex. Nat Neurosci 8:1110–1116.

851 Berger TK, Perin R, Silberberg G, Markram H (2009) Frequency-dependent
852 disynaptic inhibition in the pyramidal network: a ubiquitous pathway in
853 the developing rat neocortex. J Physiol (Lond) 587:5411–5425.

854 Bonds AB (1989) Role of inhibition in the specification of orientation selectivity
855 of cells in the cat striate cortex. Vis Neurosci 2:41–55.

856 Brascamp JW, Klink PC, Levelt WJM (2015) The "laws" of binocular rivalry: 50
857 years of Levelt's propositions. Vision Res 109:20–37.

858 Brascamp JW, van Ee R, Noest AJ, Jacobs RH, van den Berg AV (2006) The time
859 course of binocular rivalry reveals a fundamental role of noise. Journal of
860 Vision 6:1244–1256.

861 Curtu R, Shpiro A, Rubin N, Rinzel J (2008) Mechanisms for Frequency Control in
862 Neuronal Competition Models. SIAM J Appl Dyn Syst 7:609–649.

863 Delgado JY, Gómez-González JF, Desai NS (2010) Pyramidal neuron conductance
864 state gates spike-timing-dependent plasticity. J Neurosci 30:15713–
865 15725.

866 Destexhe A, Rudolph M, Fellous J-M, Sejnowski TJ (2001) Fluctuating synaptic
867 conductances recreate in vivo-like activity in neocortical neurons.
868 Neuroscience 107:13–24.

869 Dong H, Shao Z, Nerbonne JM, Burkhalter A (2004) Differential depression of
870 inhibitory synaptic responses in feedforward and feedback circuits
871 between different areas of mouse visual cortex. J Comp Neurol 475:361–
872 373.

873 Hayden BY, Moreno-Bote R (2018) A neuronal theory of sequential economic
874 choice. Brain Neurosci Adv 2:2398212818766675.

875 Heuer H (1987) Visual discrimination and response programming. Psychol Res
876 49:91–98.

877 Hodgkin AL, Huxley AF (1952) A quantitative description of membrane current
878 and its application to conduction and excitation in nerve. J Physiol
879 117:500–544.

880 Huguet G, Rinzel J, Hupé J-M (2014) Noise and adaptation in multistable
881 perception: noise drives when to switch, adaptation determines percept
882 choice. J Vis 14:19.

883 Kapfer C, Glickfeld LL, Atallah BV, Scanziani M (2007) Supralinear increase of
884 recurrent inhibition during sparse activity in the somatosensory cortex.
885 Nat Neurosci 10:743–753.

886 Kemenes I, Marra V, Crossley M, Samu D, Staras K, Kemenes G, Nowotny T (2011)
887 Dynamic clamp with StdpC software. Nat Protoc 6:405–417.

888 Kim Y-J, Grabowecky M, Suzuki S (2006) Stochastic resonance in binocular
889 rivalry. Vision Res 46:392–406.

890 Kogo N, van Ee R (2015) Neural mechanisms of figure-ground organization:
891 Border-ownership, competition and perceptual switching. In: Oxford
892 Handbook of Perceptual Organization, pp 342–362. Oxford: Oxford
893 University Press.

894 Laing CR, Chow CC (2002) A spiking neuron model for binocular rivalry. Journal
895 of Computational Neuroscience 12:39–53.

896 Lankheet MJM (2006) Unraveling adaptation and mutual inhibition in perceptual
897 rivalry. J Vis 6:304–310.

898 Lee DK, Itti L, Koch C, Braun J (1999) Attention activates winner-take-all
899 competition among visual filters. Nat Neurosci 2:375–381.

900 Leopold, Logothetis (1999) Multistable phenomena: changing views in
901 perception. Trends Cogn Sci (Regul Ed) 3:254–264.

902 Levelt WJ (1967) Note on the distribution of dominance times in binocular
903 rivalry. Br J Psychol 58:143–145.

904 Levelt WJM (1965) On binocular rivalry. Soesterberg, The Netherlands: Institute
905 for Perception RVO-TNO. Available at:
906 http://www.mpi.nl/world/materials/
907 publications/levelt/Levelt_Binocular_Rivalry_1965.pdf.

908 Lien C-C, Jonas P (2003) Kv3 potassium conductance is necessary and kinetically
909 optimized for high-frequency action potential generation in hippocampal
910 interneurons. J Neurosci 23:2058–2068.

911 Machens CK, Romo R, Brody CD (2005) Flexible control of mutual inhibition: a
912 neural model of two-interval discrimination. Science 307:1121–1124.

913 Mark S, Romani S, Jezek K, Tsodyks M (2017) Theta-paced flickering between
914 place-cell maps in the hippocampus: A model based on short-term
915 synaptic plasticity. Hippocampus 27:959–970.

916 Markram H, Toledo-Rodriguez M, Wang Y, Gupta A, Silberberg G, Wu C (2004)
917 Interneurons of the neocortical inhibitory system. Nat Rev Neurosci
918 5:793–807.

919 Masquelier T, Guyonneau R, Thorpe SJ (2009) Competitive STDP-based spike
920 pattern learning. Neural Comput 21:1259–1276.

921 Matsuoka K (1984) The dynamic model of binocular rivalry. Biol Cybern 49:201–
922 208.

923 Mikami A, Newsome WT, Wurtz RH (1986) Motion selectivity in macaque visual
924 cortex. I. Mechanisms of direction and speed selectivity in extrastriate
925 area MT. J Neurophysiol 55:1308–1327.

926 Miles R (1990) Synaptic excitation of inhibitory cells by single CA3 hippocampal
927 pyramidal cells of the guinea-pig in vitro. J Physiol 428:61–77.

928 Molnár G, Oláh S, Komlósi G, Füle M, Szabadics J, Varga C, Barzó P, Tamás G
929 (2008) Complex events initiated by individual spikes in the human
930 cerebral cortex. PLoS Biol 6:e222.

931 Moreno-Bote R, Rinzel J, Rubin N (2007) Noise-induced alternations in an
932 attractor network model of perceptual bistability. J Neurophysiol
933 98:1125–1139.

934 Moreno-Bote R, Shpiro A, Rinzel J, Rubin N (2010) Alternation rate in perceptual
935 bistability is maximal at and symmetric around equi-dominance. J Vis
936 10:1.

937 Mueller TJ (1990) A physiological model of binocular rivalry. Visual
938 Neuroscience 4:63–73.

939 Naber M, Frässle S, Einhäuser W (2011) Perceptual Rivalry: Reflexes Reveal the
940 Gradual Nature of Visual Awareness. PLoS ONE 6:e20910.

941 Noest AJ, van Ee R, Nijs MM, van Wezel RJ (2007) Percept-choice sequences
942 driven by interrupted ambiguous stimuli: a low-level neural model.
943 Journal of Vision 7:10 1-14.

944 Nowotny T, Szucs A, Pinto RD, Selverston AI (2006) StdpC: a modern dynamic
945 clamp. J Neurosci Methods 158:287–299.

946 Pastukhov A, Braun J (2011) Cumulative history quantifies the role of neural
947 adaptation in multistable perception. Journal of Vision 11 Available at:
948 http://www.journalofvision.org/content/11/10/12.abstract [Accessed
949 October 10, 2011].

950 Pelkey KA, Chittajallu R, Craig MT, Tricoire L, Wester JC, McBain CJ (2017)
951 Hippocampal GABAergic Inhibitory Interneurons. Physiol Rev 97:1619–
952 1747.

953 Pisarchik AN, Jaimes-Reátegui R, Magallón-García CDA, Castillo-Morales CO
954 (2014) Critical slowing down and noise-induced intermittency in bistable
955 perception: bifurcation analysis. Biol Cybern 108:397–404.

956 Pospischil M, Toledo-Rodriguez M, Monier C, Piwkowska Z, Bal T, Frégnac Y,
957 Markram H, Destexhe A (2008) Minimal Hodgkin-Huxley type models for
958 different classes of cortical and thalamic neurons. Biol Cybern 99:427–
959 441.

960 Ren M, Yoshimura Y, Takada N, Horibe S, Komatsu Y (2007) Specialized
961 inhibitory synaptic actions between nearby neocortical pyramidal
962 neurons. Science 316:758–761.

963 Said CP, Heeger DJ (2013) A Model of Binocular Rivalry and Cross-orientation
964 Suppression. PLOS Computational Biology 9:e1002991.

965 Seely J, Chow CC (2011) Role of mutual inhibition in binocular rivalry. Journal of
966 Neurophysiology 106:2136–2150.

967 Shpiro A, Curtu R, Rinzel J, Rubin N (2007) Dynamical characteristics common to
968 neuronal competition models. J Neurophysiol 97:462–473.

969 Shpiro A, Moreno-Bote R, Rubin N, Rinzel J (2009) Balance between noise and
970 adaptation in competition models of perceptual bistability. J Comput
971 Neurosci 27:37–54.

972 Silberberg G, Grillner S, Lebeau F, Maex R, Markram H (2005) Synaptic pathways
973 in neural microcircuits. Trends in Neurosciences 28:541–551.

974 Silberberg G, Markram H (2007) Disynaptic inhibition between neocortical
975 pyramidal cells mediated by Martinotti cells. Neuron 53:735–746.

976 Sillito AM (1975) The contribution of inhibitory mechanisms to the receptive
977 field properties of neurones in the striate cortex of the cat. J Physiol
978 250:305–329.

979 Snowden RJ, Treue S, Erickson RG, Andersen RA (1991) The response of area MT
980 and V1 neurons to transparent motion. J Neurosci 11:2768–2785.

981 Tremblay R, Lee S, Rudy B (2016) GABAergic Interneurons in the Neocortex:
982 From Cellular Properties to Circuits. Neuron 91:260–292.

983 Uhlenbeck GE, Ornstein LS (1930) On the Theory of the Brownian Motion. Phys
984 Rev 36:823–841.

985 Usher M, McClelland JL (2001) The time course of perceptual choice: the leaky,
986 competing accumulator model. Psychol Rev 108:550–592.

987 Wang C-T, Lee C-T, Wang X-J, Lo C-C (2013) Top-down modulation on perceptual
988 decision with balanced inhibition through feedforward and feedback
989 inhibitory neurons. PLoS ONE 8:e62379.

990 Wang Q, Burkhalter A (2007) Area map of mouse visual cortex. Journal of
991 Comparative Neurology 502:339–357.

992 Wilson HR (1999) Spikes, Decisions, and Actions: The Dynamical Foundations of
993 Neuroscience, Pap/Dskt/C edition. Oxford ; New York: Oxford University
994 Press.

995 Wilson HR, Krupa B, Wilkinson F (2000) Dynamics of perceptual oscillations in
996 form vision. Nat Neurosci 3:170–176.

997 Zhou H, Friedman HS, von der Heydt R (2000) Coding of border ownership in
998 monkey visual cortex. Journal of Neuroscience 20:6594–6611.

999

1000 **Figure legends**

1001 **Figure 1.** Mutual inhibition circuit and experimental design. **a**: Neural circuit
1002 diagram for a mutual inhibition. Triangles: pyramidal neurons (PNs). Disks:
1003 inhibitory neurons (INs). **b**: The disynaptic mutual inhibition circuit was
1004 established between two real-life pyramidal neurons by implementing model
1005 inhibitory neurons and synapses (dashed lines) in the StdpC dynamic clamp
1006 system. **c**: An image of the brain slice (right hemisphere) from a DIC-IR
1007 microscope during recording with two patch recording pipettes placed in layer
1008 2/3 of V1. 1 to 6: six layers. LM: lateromedial area. d: dorsal, v: ventral, l: lateral,
1009 m: medial. Scale bar: 200 μm. **d**: An example of biocytin filled pair of pyramidal
1010 neurons. Scale bar: 50 μm.

1011

1012 **Figure 2.** Mutual inhibition between a pair of pyramidal neurons **a**: An action
1013 potential in PN1 (red triangle) evoked EPSPs in the partner model inhibitory
1014 neuron (mIN1). The synaptic events in mIN1 are shown with six different levels
1015 of model synaptic conductance. With the higher synaptic strength, the EPSP
1016 evoked an action potential in mIN1 (red disks) causing evoked IPSP in the target
1017 pyramidal neuron, PN2 (blue asterisks). When the synaptic strength is in the

lower range, it only evoked an EPSP without an action potential in mIN1 (#) and, hence, without an IPSP in PN2. Vice versa from PN2 to mIN2 and PN1. **b**: The activities of PNs and mINs during bi-stable activity.

Figure 3. Computation of dominant durations. **a**: A part of a recording of bi-stable activity. **b**: First step computation of dominance durations. Here, continuous firing of action potentials in one neuron until an action potential occurs in the other neuron is considered as a tentative dominance duration of the first neuron. Hence, the dominant durations of the two neurons are mutually exclusive. Note that there are short dominant durations (blue asterisks for PN2 and red asterisk for PN1). There are also series of alternations of short dominant durations between the two neurons (green asterisks). **c**: Dominance durations after choosing only long durations (longer than 250 ms). This process results in short lags between the dominance durations (blue and red asterisks). There are also the intervals that are not assigned to either of the neurons corresponding to the period marked with green asterisks in **b**. The short lags are not considered as reversals and, hence, the previous dominance is considered to continue (arrows). **d**: These processes result in the final dominance durations without short durations. And the periods not assigned to neither of the neurons are assigned as “both active” (bottom).

Figure 4. **a**: Inter-spike intervals of an example shown in Figure 5a. **b**: Linear regression (black) of inter-spike intervals (orange plot) taken from the first cycle of PN1 (orange asterisk in **a**) plotted over time from the onset of its dominance duration.

Figure 5. Evoked bi-stable activity in a pair of pyramidal neurons with mutual inhibition connections. **a**: Continuous injection of depolarization currents into the two pyramidal neurons produces bi-stable activity with alternating dominance between them. MP: membrane potential (mV). MC: membrane current (pA). Inset: The response of the same pyramidal neurons to the same depolarization current injection without the mutual inhibition circuit, showing sustained continuous firing of action potentials. **b**: The part of data (orange rectangle) shown in **a**. Upon the onset of the current injection, both neurons started to depolarize, but fired an action potential first. As a result, PN1 received an IPSP causing PN2 to become dominant and PN1 suppressed. **c**: The part of data (orange triangle) around the time of reversal. The inter-spike interval increased during the dominant period of PN2 due to adaptation. Just after the rightmost action potential of PN2, PN1 got a sufficient time to recover from its IPSP, enabling it to reach its firing threshold before PN2 was able to fire its next action potential. The action potential of PN1 now resulted in an IPSP in PN2 entailing a reversal of dominance.

Figure 6. Adaptation of dominant neuron and its correlation to dominance duration. **a-b**: The physiological signatures of adaptation. Inter-spike intervals increase (**a**) and the peaks of action potentials decrease (**b**) due to adaptation during dominance episodes. **c-d**: Average of inter-spike intervals (**c**) and the action potential peaks (**d**) for pooled data of all 93 “control pairs” (see Methods for the definition). **e**: Slope of inter-spike interval as a function of dominance durations, showing the inverse correlation between them. **f**: Inverse correlation

between the slope of inter-spike interval and dominance duration in the pooled data. The dominance durations of individual pairs were normalized by their mean values before pooling. The normalized duration was binned and the pooled data was averaged for the individual bins. Error bars indicate +/- SEM.

Figure 7. Effect of adding noise. Model excitatory and inhibitory synaptic noise was applied to the pyramidal neurons and the inhibitory neurons through the dynamic clamp system. **a-b**: Baseline membrane potentials at -60mV without (**a**) and with (**b**) the model noise. **c**: Effect of changing the noise level systematically to bi-stable activity. Increase of the noise resulted in increase of reversal rate (from top to bottom). Noise levels are indicated as standard deviations (SD) of gE and gI (excitatory and inhibitory conductance, respectively, in nS). Asterisk: Data with the "standard" noise parameter set. **d**: Pooled data of the effect of noise (N=15). The reversal rates from the individual pair are normalized by the value at the standard noise parameters (iii) before pooling. Orange bar (i) indicates the data with no model noise. Error bars indicate +/- SEM. The noise parameter sets for i (no model noise), ii, iii (standard noise parameters), iv and v are shown in the table below. The noise level is increased linearly from ii to v. **e**: Histogram of dominance durations for PN1 and PN2 from 10 minutes continuous recording (with the "standard" noise parameters).

Figure 8. Schematics of experimental paradigm and the result. **a**: Schematics of the paradigms equivalent to Levelt's experimental paradigms for bi-stable perception. The level of injected current to either one or both of the two mutually inhibiting pyramidal neurons was systematically changed (analogous

to the change of the contrasts in Levelt's experiments). **b**: Example data of the experiment equivalent to the generalized Levelt's experimental paradigm for proposition I to III. The level of depolarization current in PN1 was increased (from top to bottom) while the current to PN2 was kept constant. **c-e**: Changes in dominance (**c**), dominance duration (**d**), and reversal rate (**e**) for this pair. PN1 red, PN2 blue. **f-h**: Pooled data (N=46) plotted over the normalized injected current. The dominance durations are normalized for the maximum values of the individual neurons. Red: responses of the neurons that received the changes of the injected current. Blue: responses of the neurons whose injected current was kept constant. Left column: The data of the individual pairs. Right column: The normalized current was binned and the pooled data were averaged for the individual bins. Error bars indicate +/- SEM.

Figure 9. Examples of responses of average durations and reversal rate (shown in non-normalized absolute values) to the change of the depolarization current to one of the pair of pyramidal neurons (red) while the current to the other neurons was kept constant (blue). **a-c**: The example pairs where the reversal rates decreased when the current either increased or decreased from the control value ($I_{50\%}$). **d-f**: The examples where the reversal rates increased when the current increased from the control value ($I_{50\%}$). Note that, in the latter case, the increase of the average.

Figure 10. Results of experimental paradigm equivalent to the generalized Levelt's paradigm for proposition IV. **a**: The effect of increasing the depolarization currents simultaneously in both pyramidal neurons (from top to

bottom). **b**: The changes of the reversal rate for this pair. **c**: Pooled data of reversal rate (N=32) plotted over the normalized injected currents.

Figure 11. Effect of short-term depression on bi-stable activity. **a**: Depression of EPSPs evoked by a train of modelled presynaptic spikes (by Spike Generator, SG, at 40Hz). g_{syn} was set to 5nS to avoid generation of action potentials for illustration purposes. **b**: A disynaptic inhibitory circuit was established between SG, model inhibitory neurons (mINs) and real-life pyramidal neurons (PNs) as illustrated in the schematic at the top. The membrane potentials of PNs were set to -60mV to make IPSPs visible. Three different conditions were tested, including no STD (top), STD with strong (g_{syn}=50nS, middle) and weak (g_{syn}=20nS, bottom) synapses in both the inhibitory and excitatory connections. A train of ten spikes was generated in the SG at 20Hz. Without STD, all ten EPSPs successfully evoked action potentials in INs (left column). These action potentials, in turn, evoked long lasting IPSPs in PNs (right column). With STD (strong and weak synaptic strength, middle and bottom traces, respectively), the gradual decrease of EPSP size caused failures of evoking action potentials in INs (asterisks), resulting in weaker IPSPs in the target PNs. **c**: An example of the effect of STD on bi-stable activity. Without STD (top trace), with STD with strong synapses (middle traces) and with weak synapses (bottom traces). With STD with strong synapses, action potentials in the dominant PN soon failed to evoke action potentials in the connected IN due to the depression of EPSPs and reversal of dominance occurred quickly. With STD with weak synapses, EPSPs evoked by action potentials in PNs failed to evoke action potentials in INs most of the time, neither of the PNs was

1142 able to establish dominance, and both PNs showed continuous firing of action
1143 potentials independently.
1144
1145 **Tables**
1146 **Table 1** Parameter sets for modelled ionic channels (top), synaptic
1147 conductance (middle) and synaptic noise (bottom).
1148

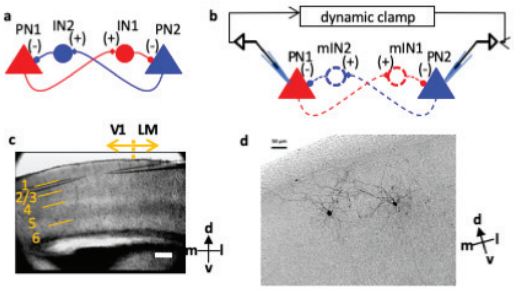

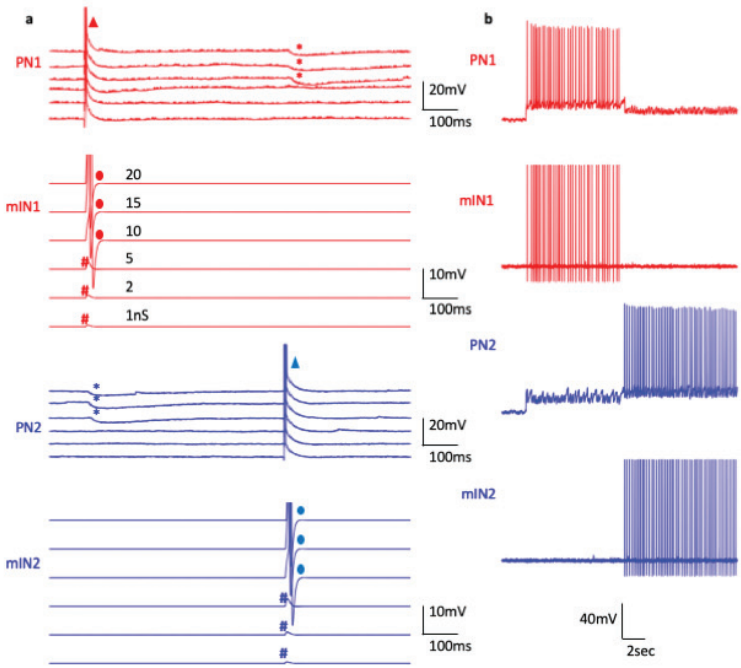

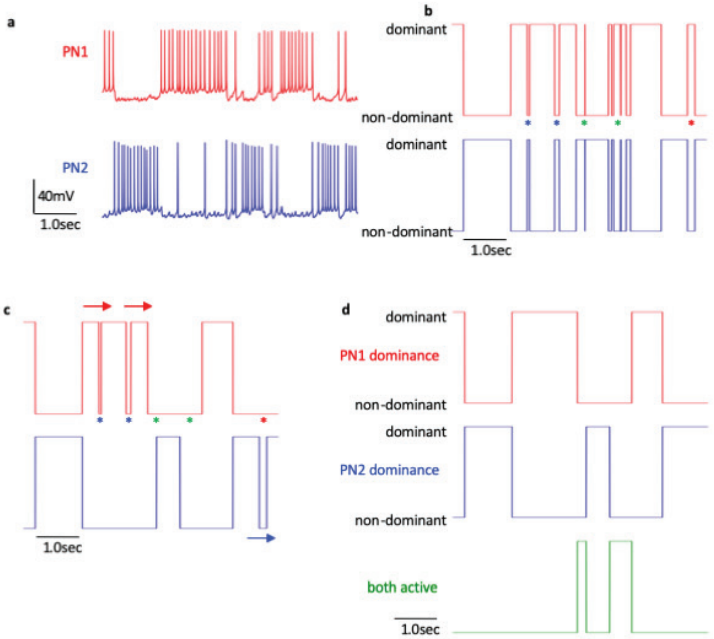

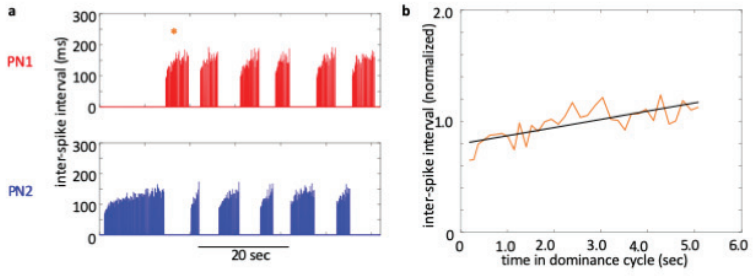

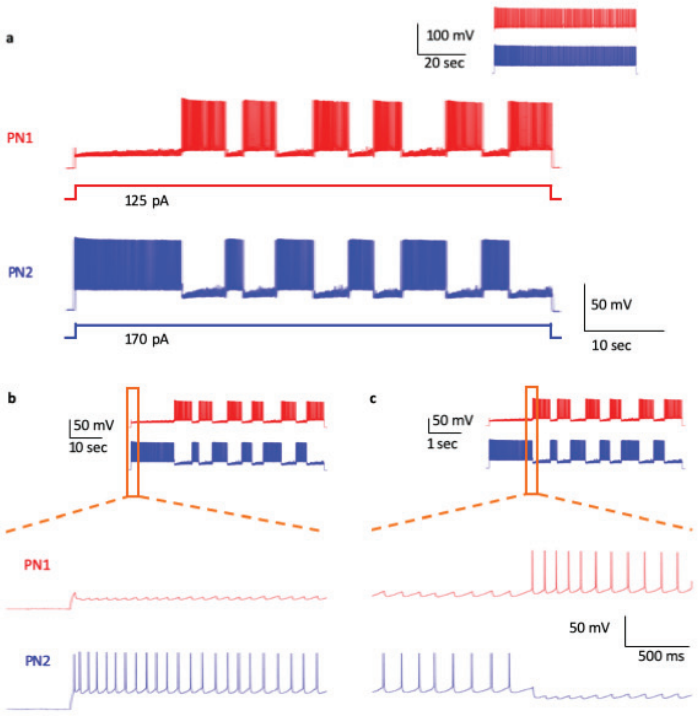

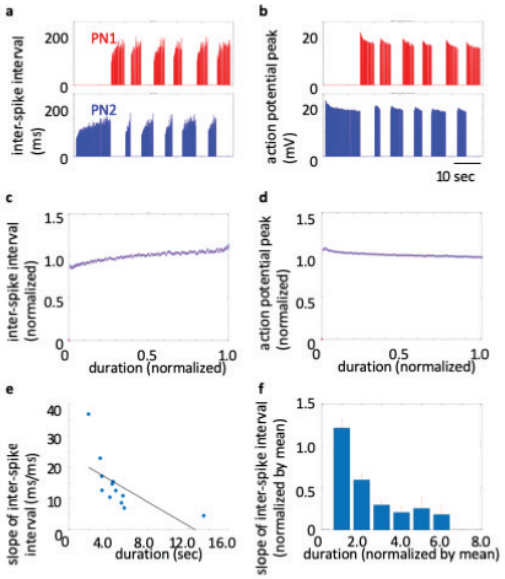

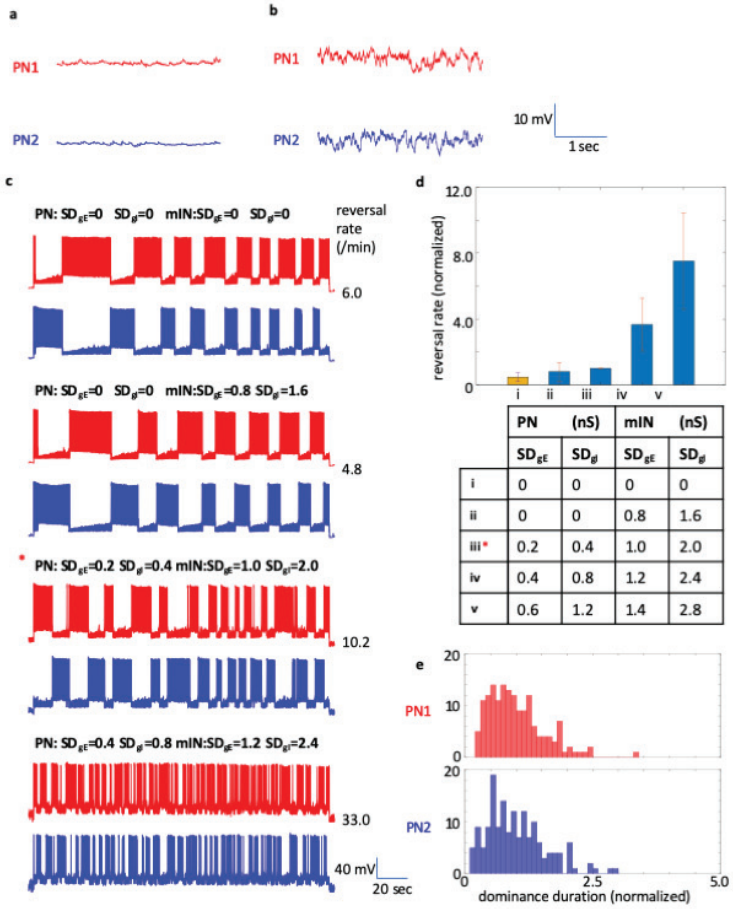

	PN (nS)		mIN (nS)	
	SD_{gE}	SD_{gI}	SD_{gE}	SD_{gI}
i	0	0	0	0
ii	0	0	0.8	1.6
iii*	0.2	0.4	1.0	2.0
iv	0.4	0.8	1.2	2.4
v	0.6	1.2	1.4	2.8

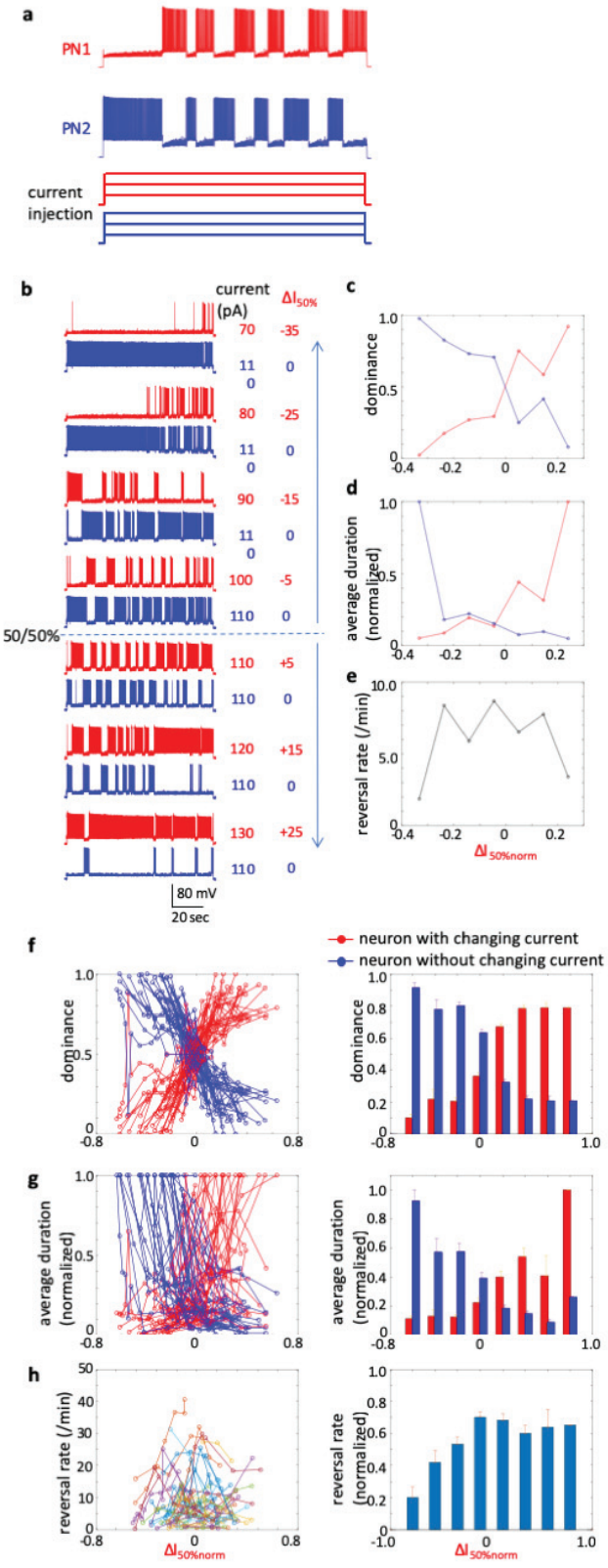

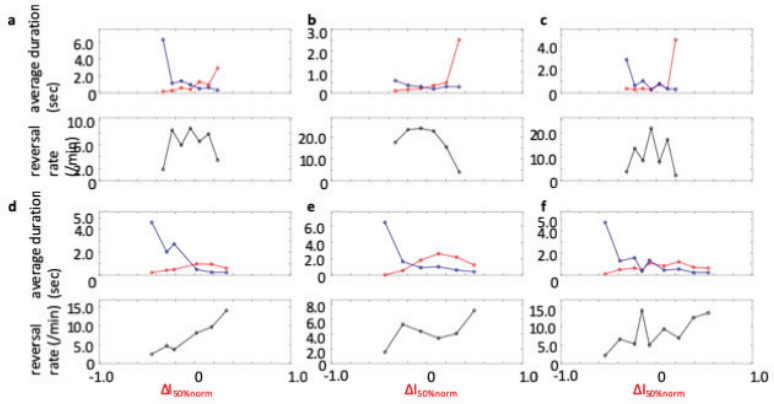

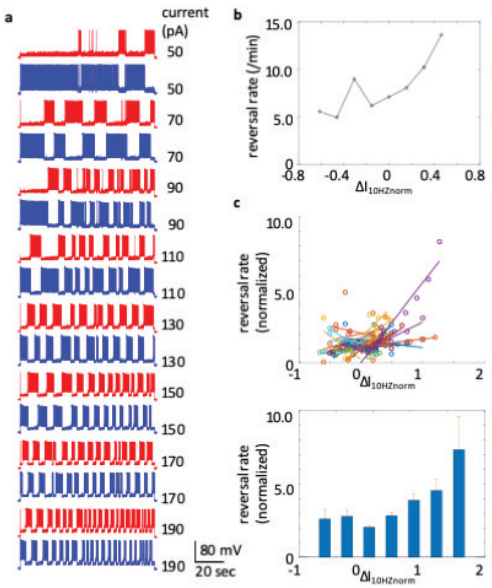

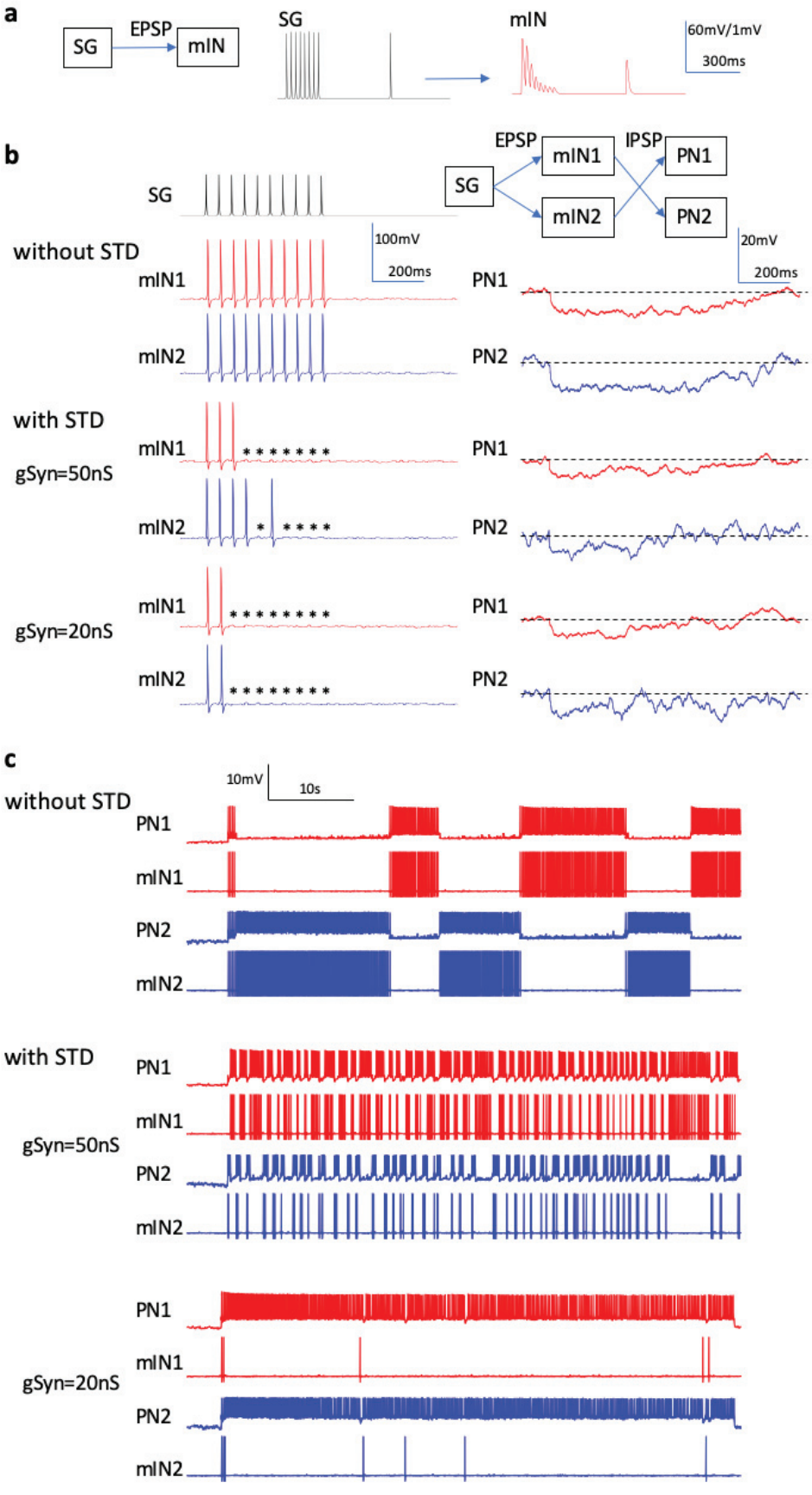

parameters for ionic channel models

	g_{max} (nS)	V_{rev} (mV)		exponential	α/β	F	k (1/ms)	$V_{\_,\_}$ (mV)	S (mV)
Na	25385	50	activation	3	α	1	1.0	-40	-10
					β	2	4.0	-65	-18
			inactivation	1	α	2	0.07	-65	-20
					β	3	1.0	-35	-10
K_d	615	-100	activation	4	α	1	0.1	-55	-10
					β	2	0.125	-65	-80
K_{V3}	3000	-100	activation	1	α	1	-0.12166	4.18371	-6.42606
					β	2	0.015857	0	-25.4834

parameters for synapse models

	g_{syn} (nS)	V_{syn} (mV)	τ_{syn} (ms)	V_{TH} (mV)	V_{slope} (mV)	synaptic delay (ms)
excitatory	10	0	5	-20	25	1.0
inhibitory	10	-70	100	-20	25	1.0

parameters for synaptic noise model

		g_{mean} (nS)	SD_g (nS)	V_{rev} (mV)	τ (ms)
PN	excitatory	0	0.2	0	5
	inhibitory	0	0.4	-70	10
IN	excitatory	2	1.0	0	5
	inhibitory	10	2.0	-70	10